Proceedings of the Seventh International Conference on
Railway Technology: Research, Development and Maintenance
Edited by: J. Pombo
Civil-Comp Conferences, Volume 15, Paper 11.10
Civil-Comp Press, Edinburgh, United Kingdom, 2026
ISSN: 2753-3239, doi: 10.4203/ccc.15.11.10

Numerical Studies on Aerothermal Characteristics and Mitigation Strategies for Vacuum Tube Transportation

Y. Bi[1], H. Bi[2], H. Wang[1] and W. Luo[1]

[1]School of Mechanical Engineering, Southwest Jiaotong University, Chengdu, China
[2]Research Center for Super-High-Speed Evacuated Tube Maglev Transport, Southwest Jiaotong University, Chengdu, China

Abstract

The Vacuum Tube Maglev Transportation System, as a crucial development trend in the future transportation sector, has a special enclosed environment that renders the thermal environment within the tube highly complex and even endangers operational safety. Thus, an investigation into the formation mechanisms of aerodynamic heat provides technical support for its engineering application. This paper studies aerodynamic heat using the Shear Stress Transport *k-ω* model, combined with the dynamic mesh technique. To mitigate the transient aerodynamic heating caused by train operation, an aerodynamic heating mitigation scheme based on the heat dissipation method of cold radiant panels is proposed, and the mitigation effect of the cold radiant panel area on transient aerodynamic heating is discussed. The key result is that when the cold radiant panels are fully laid along the entire length of the tube, the maximum temperature on the train surface is 12.4 °C lower than that without the cold radiant panels.

Keywords: vacuum tube, maglev train, ultra-high-speed, aerodynamic heat, thermal environment, shock wave.

1 Introduction

The development of railways has been intertwined with the tremendous progress of human transportation—each technological breakthrough in rail systems, from electrification to vacuum tube maglev, has pushed the boundaries of how people and goods move across distances [1]. However, the high-velocity flow field surrounding the train generated by its supersonic operation induces flow phenomena such as turbulence, shock waves, and expansion waves. These phenomena drive intense friction and result in the generation of substantial aerodynamic heat [2].

At present, some scholars have mainly studied the aerothermal characteristics of vacuum tube trains. According to their investigations, critical parameters such as the system blocking ratio [3,4], train velocity [5], vacuum degree [6], train configuration [7], and initial ambient temperature [8] exert substantial influences on the aerodynamic heating behaviour of vacuum tube transport systems. Specifically, Li et al. [9] investigated the aerodynamic heating phenomenon arising from high-speed train operation via scaled model experiments. Their results show that heat is distributed non-uniformly within the tube, leading to a rise in internal air temperature and heating of both the train surface and tube wall, which in turn intensifies the corresponding heat transfer processes. Yu et al. [10,11] studied thermal effects in choked and unchoked flows in the tube and analyzed the thermal load distribution on the train and tube walls. Hu et al. [12] pointed out that lowering the pressure within the vacuum tube system leads to a weakening of both radiative and convective heat transfer of air. For aerodynamic heat mitigation strategies, some scholars [13,14,15] investigated the effects of different streamlined head lengths on aerodynamic characteristics and in-tube temperature. They found that the nose shape of the head has a significant influence during train acceleration and deceleration, and the wave system and temperature field around the train tail are even more strongly affected by the nose configuration. Xie et al. [16] investigated the aerodynamic heating of evacuated tube transportation under choked flow conditions, considering the coupled effect of forced convection and surface radiation, in contrast to existing studies that only analyze single heat transfer modes and flow structures.

Based on a prototype of an actual engineering train, this paper establishes a three-dimensional numerical model of the vacuum tube train and conducts a study on transient aerodynamic heating and corresponding mitigation strategies. This paper can provide a useful reference for the future engineering design of evacuated tube maglev transportation systems. This paper consists of five parts and is structured as follows: Section 2 introduces the geometric model, boundary conditions, numerical mesh, flow control equations, validation, and heating mitigation design. Section 3 presents the flow and heat transfer characteristics within the tube and discusses the effect of cold radiant panels on mitigating the aerodynamic heat. Finally, Section 4 summarizes the main research conclusions.

2 Methods

2.1 Geometric model for the maglev train and tube

A 1:1 three-dimensional numerical model of a three-train maglev train, based on a specific practical project, is established in this study and presented in Fig. 1. The train has an overall length (H_L) of 62 m, a width (H_W) of 2.9 m, and a height (H_R) of 3.7 m. The vacuum tube has a radius of 3 m, corresponding to a blockage ratio of 0.36.

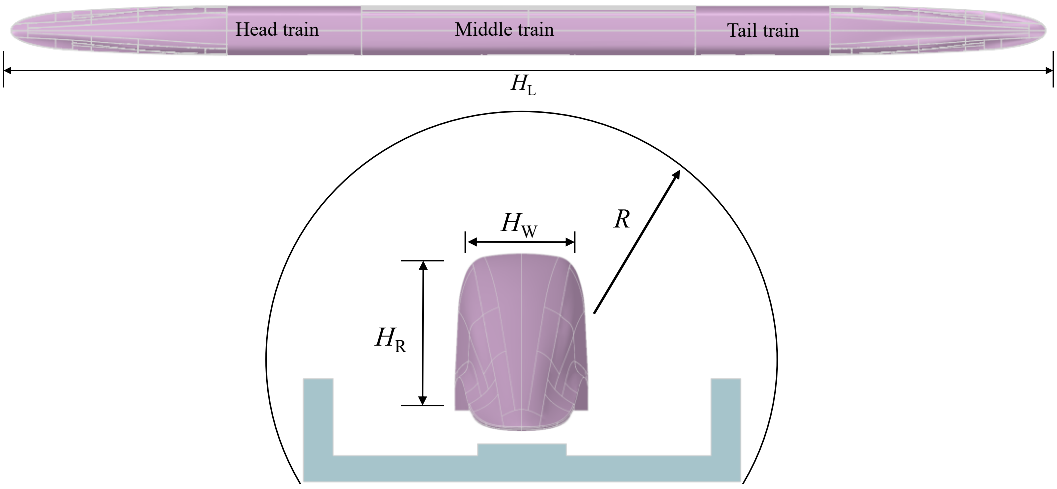

Figure 1: The configuration of the evacuated tube maglev transportation system.

2.2 Boundary conditions

The total length of the computational domain is set to 352.2 H_R, which is considerably shorter than the actual tube length in real engineering applications. To suppress wave reflections at the boundaries, both ends of the tube are specified as pressure far-field conditions, enabling an approximation of an infinitely long vacuum tube. As shown in Fig. 2, the initial distances from the train to the upstream and downstream boundaries are 27 H_R and 308.5 H_R, respectively. The surfaces of the tube, track supports, and train body are defined as adiabatic no-slip walls. The ambient static temperature and static pressure inside the tube are initialized at 300 K and 1013.25 Pa, and the train travels at a speed of 1200 km/h.

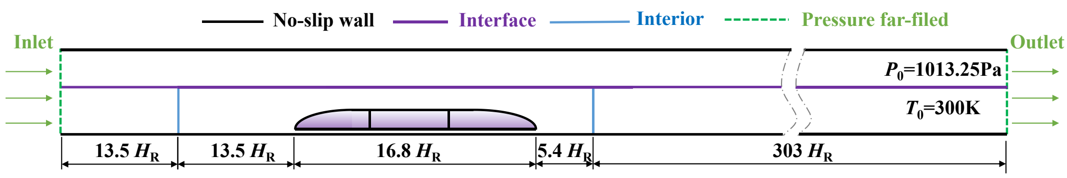

Figure 2: The computational domain and boundary conditions.

2.3 Mesh strategy

For the purpose of capturing the velocity gradient and flow characteristics near the train with higher accuracy, and further conducting precise analysis of aerothermal effects, flow separation, and transition behaviours, a tetrahedral mesh size of 0.05 m is adopted for the train surface, paired with a 15-layer boundary layer grid. This configuration ensures that the train's y+ is below 1. The prismatic mesh size for the front and behind domains is set to 0.2 m, while the tetrahedral mesh size of the train's computational domain is 0.1 m. Simultaneously, to guarantee adequate heat transfer between the fluid and the tube, boundary layer grids are additionally partitioned at the fluid-solid interface. The total number of meshes is 13.9×10^6. Figure 3 shows the mesh strategy.

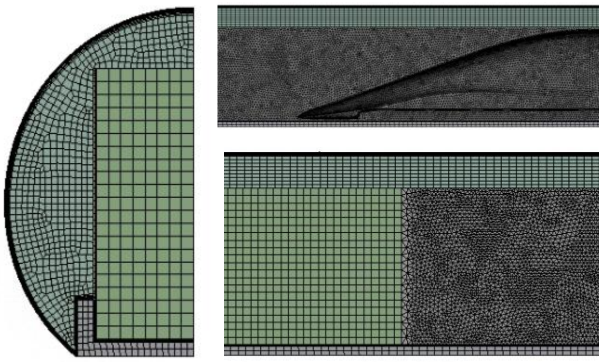

Figure 3: Mesh strategy.

2.4 Numerical model

When a train travels at ultra-high speed inside a vacuum tube, the Mach number exceeds 0.3. It is necessary to consider the gas compressibility. The flow is governed by the mass conservation equation, the momentum conservation equation, the energy conservation equation, and the ideal state equation. These relevant governing equations are as follows [1,4]:

$$\frac{\partial \rho}{\partial t} + div(\rho u) = 0 \tag{1}$$

$$\frac{\partial(\rho T)}{\partial t} + div(\rho u T) = div\left[\frac{h}{c_p} gradT\right] + S_T \tag{2}$$

$$\frac{\partial(\rho u)}{\partial t} + div(\rho u u_i) = -\frac{\partial p}{\partial x_i} + div(\mu gradu_i) + S_i \tag{3}$$

$$p = \rho R T \tag{4}$$

where ρ, t, u, u_i, T, h, c_p, μ, S_T, x_i, S_i, p, and R are the density, the time, airflow velocity vector, components of the velocity vector in different directions, heat transfer coefficient, specific heat capacity, coefficient of viscosity, viscous dissipation source in different directions, the pressure, the ideal gas constant, and generalized source term of the momentum conservation equation.

Meanwhile, Radiation effects must be considered in the analysis of aerodynamic heating. Herein, this study adopts the DO radiation model, and the standard radiation transfer equation can be expressed as:

$$\frac{dI(\vec{r},\vec{s})}{ds} + \left(a + \sigma_s\right) I(\vec{r},\vec{s}) = an^2 \frac{\sigma T^4}{\pi} + \frac{\sigma_s}{4\pi} \int_0^{4\pi} I\left(\vec{r},\vec{s}'\right) \Phi\left(\vec{s}\cdot\vec{s}'\right) d\Omega' \tag{5}$$

where $\vec{r}$ denotes the position coordinates, $\vec{s}$ represents the direction coordinates, $\vec{s}'$ stands for the direction of the scattering vector, s is the radiation path length, a

denotes the absorption coefficient, n is the refractive index, σ_s represents the scattering coefficient, σ is the Stefan-Boltzmann constant, I denotes the radiation intensity, Φ' is the phase function, and Ω' represents the solid angle.

For turbulence modelling, the SST k-ω model addresses the excessive sensitivity of the conventional k-ε model in far-wall regions and mitigates the limitations of the standard k-ω model near wall boundaries. The transport equations for the turbulent kinetic energy k and the turbulent dissipation rate ω of the SST k-ω turbulence model are [1,4]:

$$\frac{d\rho k}{dt} = \frac{\partial}{\partial x_j}\left[\left(\mu_l + \sigma_k \mu_t\right)\frac{\partial k}{\partial x_j}\right] - \beta^* \rho\omega k + \tau_{ij}\frac{\partial u_i}{\partial x_j} \tag{6}$$

$$\frac{d\rho\omega}{dt} = \frac{\partial}{\partial x_j}\left[\left(\mu_l + \sigma_\omega \mu_t\right)\frac{\partial \omega}{\partial x_j}\right] - \beta' \rho\omega^2 + \frac{\gamma'}{\nu_t}\tau_{ij}\frac{\partial u_i}{\partial x_j} + 2\left(1 - F_1\right)\rho\sigma_{\omega 2}\frac{1}{\omega}\frac{\partial k}{\partial x_j}\frac{\partial \omega}{\partial x_j} \tag{7}$$

where μ_l is the laminar flow viscosity coefficient, μ_i is the turbulent flow viscosity coefficient, τ_{ij} represents the stress tensor, and F_1 stands for the mixing function. F_1 is used to combine the advantages of the standard k-ε model and the standard k-ω model.

2.5 Validation

The numerical method is validated against experimental pressure data from the NASA Langley 8-Foot Transonic Wind Tunnel reported by Kayser & Whiton [17]. As shown in Fig. 4, the computational domain matches the wind tunnel dimensions of 2.16 × 2.16 m, with a slender SOCBT projectile of diameter $D = 0.057$ m placed 10 m from both domain boundaries. The projectile and tunnel walls are set as stationary no-slip boundaries, and a pressure far-field condition with an inlet Mach number of 1.2 is applied. Two refinement zones are employed to ensure accuracy, with a surface grid size of 0.000125 m on the projectile (Fig. 4(b)).

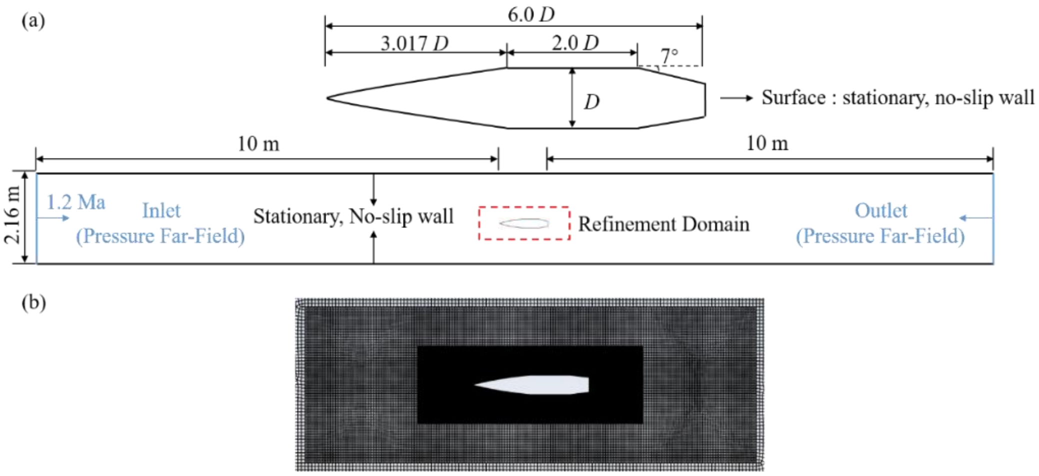

Figure 4: Schematic diagram of the size and grid of the SOCBT projectile model: (a) the computational domain; (b) the mesh of the refinement domain.

As illustrated in Fig. 5(a), the numerically predicted pressure coefficient on the projectile upper surface agrees well with experimental measurements, with a maximum discrepancy of 7%. The shock and expansion waves around the projectile are well captured in Fig. 5(b). These results confirm that the present numerical method is reliable for simulating the flow field in the vacuum tube, and its validity has also been supported by relevant literature [12,18].

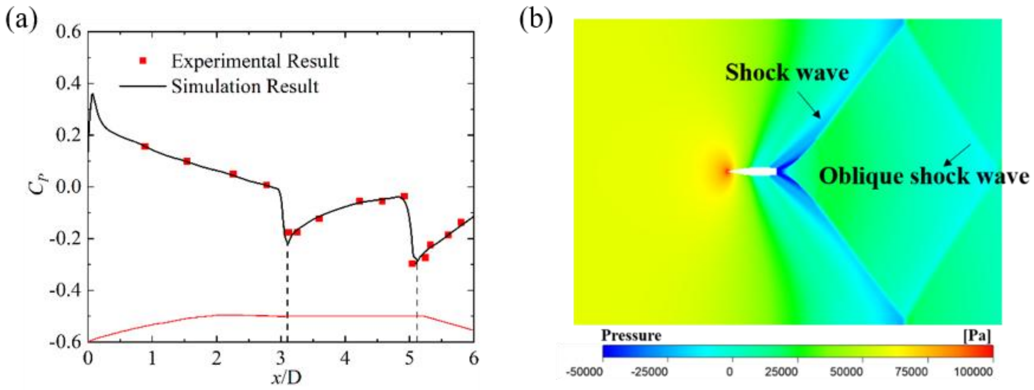

Figure 5: Validation of pressure coefficient and pressure distribution around the projectile: (a) the pressure coefficient comparison; (b) the captured aerodynamic phenomenon.

2.6 Transient Aerodynamic Heating Mitigation Design

Cold radiant panels are installed in sections along the inner wall of the vacuum tube, and their temperature is lowered by continuously circulating cooling water. This creates a temperature difference relative to the tube wall and the surrounding air, thereby removing heat from the tube.

As illustrated in Fig. 6, considering construction convenience and operational safety of the train, cold radiant panels are arranged at intervals on both sides of the track. For boundary conditions, the wall surfaces equipped with cold radiant panels are set to a constant temperature of 21.85 ℃, while the remaining wall surfaces are specified as 26.85 ℃. All other boundary conditions remain consistent with those described in Section 2.2.

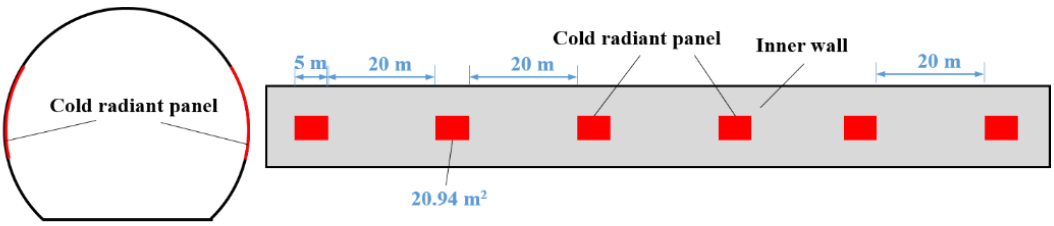

Figure 6: Schematic layout of the cold radiant panels.

3 Results

3.1 Flow and heat transfer characteristics within the tube

When a train travels at an ultra-high-speed inside an evacuated tube, the flow and heat transfer characteristics of the air around the train are presented in Fig. 7. A normal shock wave forms ahead of the train. Meanwhile, a series of expansion fans and oblique shock waves develops at the train's tail. After multiple reflections, these oblique shock waves eventually form a normal shock wave at the downstream end. While the airflow passes through the annular gap between the train and the tube, its velocity increases significantly. Once the flow reaches a critical state, further increases in the incoming velocity cannot force additional air through the annular gap, resulting in air accumulation and choked flow upstream of the train. It creates a positive pressure zone ahead of the train that propels the air forward, accompanied by a temperature rise in this region. Conversely, a negative pressure zone forms at the train's tail, drawing the airflow forward.

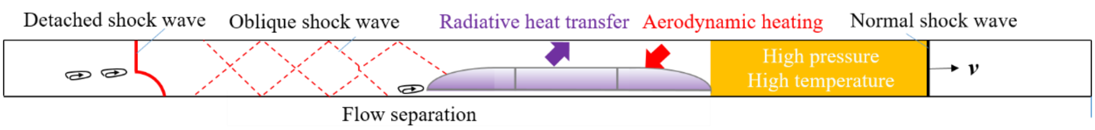

Figure 7: Flow and heat transfer characteristics of air around the train inside the tube.

Affected by viscous shear between the train surface and the tube wall, the airflow near the train moves in the forward direction, whereas the flow near the tube wall travels backward. During flow over the train surface, kinetic energy is converted into internal energy via frictional dissipation, producing high-temperature flow. Meanwhile, aerodynamic heating across shock waves further elevates the airflow temperature. This high-temperature flow continuously heats the train surface, transferring part of the energy to the train in the form of aerodynamic heating, while the remainder dissipates directly into the tube. As the train temperature rises, it subsequently releases heat to the tube wall through thermal radiation.

3.2 Mitigation effect of transient aerodynamic heating within the tube

Aiming at the transient temperature rise during the train's constant-speed operation, this section proposes a transient aerodynamic heating mitigation strategy based on the cold radiant panels cooling scheme mentioned in section 2.6, to investigate its mitigation effect on aerodynamic heating numerically.

As illustrated in Fig. 8, comparison of the temperature contours on the longitudinal section at the tube center indicates that no appreciable differences exist in the temperature and pressure distributions within the tube. This phenomenon can be attributed to the fact that the tube center section is spaced 2.5 m apart from the cold radiant panel. Under the present conditions, the temperature and surface area of the cold radiant panel are insufficient to exert a noticeable effect on the pressure and temperature fields at the relatively distant tube center longitudinal section.

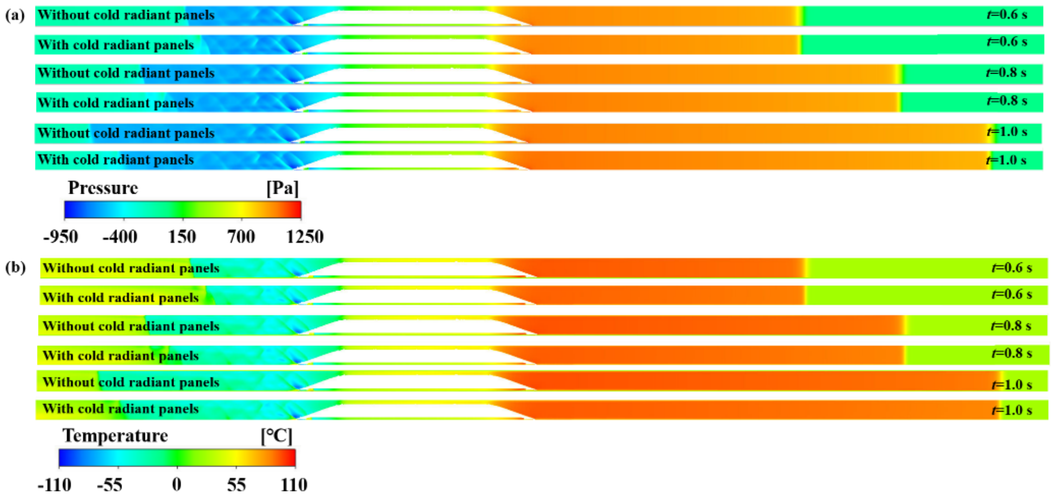

Figure 8: Pressure and temperature contours around the train with and without cold radiant panels on the tube wall.

For a qualitative analysis of the air temperature variation around the cold radiant panel, three monitoring lines L_1, L_2, and L_3 are arranged at the same horizontal plane ($y = 2.14$ m), as shown in Fig. 9. These lines are spaced 0.1 m apart from the cold radiant panel and are employed to characterize the temperature and pressure evolution at different positions within the tube space.

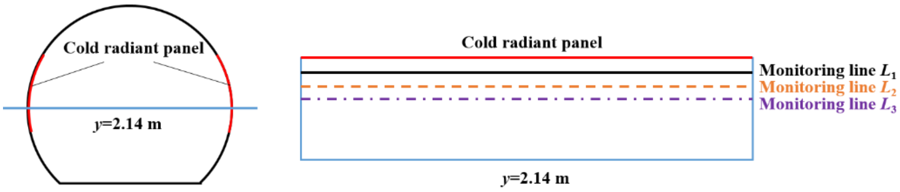

Figure 9: Schematic layout of monitoring lines inside the tube.

Figure 10 presents the temperature variations at different monitoring lines from 0.6 s to 1.0 s. It can be observed that the temperature exhibits continuous variations along each monitoring line. Moreover, as indicated by the elliptical box in the figure, temperature fluctuations in the high-temperature choked region ahead of the train become more pronounced as the distance to the cold radiant panel decreases. Meanwhile, due to the low temperature of the radiant panel, a distinct local low-temperature zone forms in the undisturbed region upstream of the high-temperature choked region. The results also show that the closer to the surface of the cold radiant panel, the more significant the temperature fluctuations in the high-temperature choked region ahead of the train and the low-temperature region behind the train. Within the annular space formed between the train and the tube, the air temperature decreases more noticeably at positions closer to the cold radiant panel. This is attributed to the smaller spatial thermal resistance between the air and the cold radiant panel at shorter distances, which enhances the intensity of radiative heat transfer.

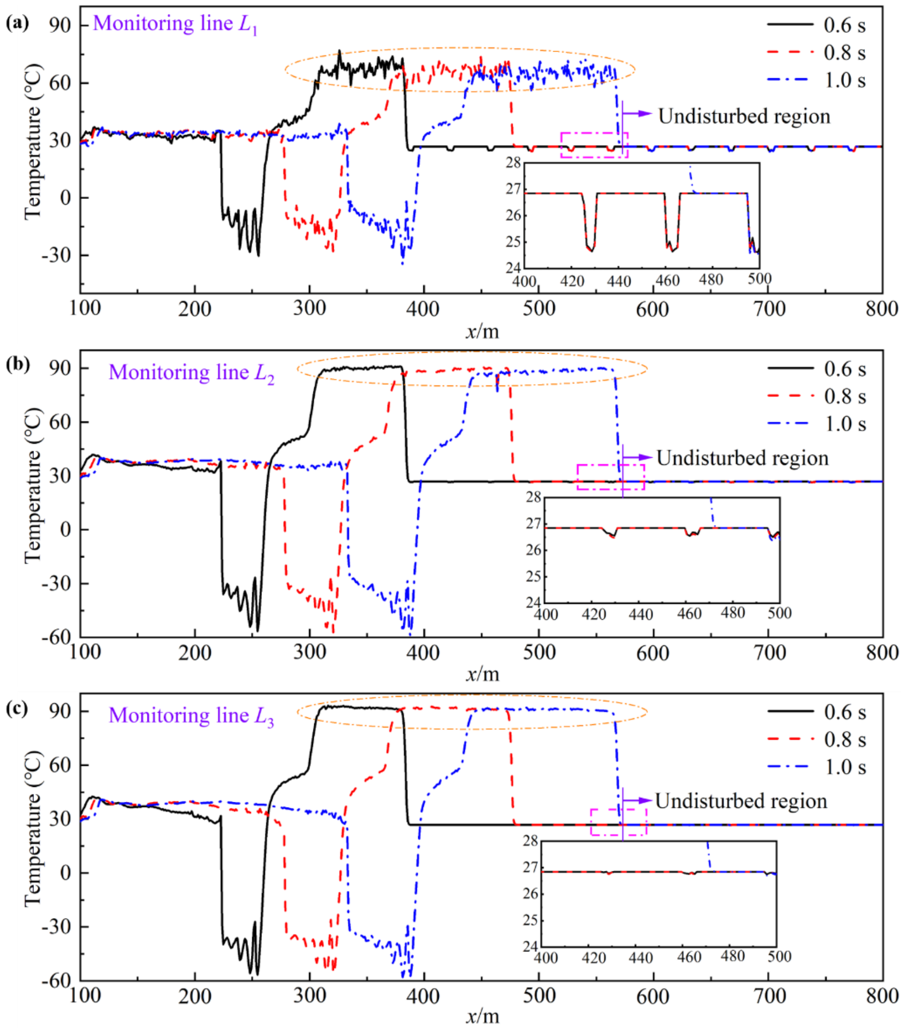

Figure 10: Temperature variations at different monitoring lines from 0.6 s to 1.0 s.

Figure 11 compares the temperature variations at different vertical positions under conditions with and without radiant cooling on the wall. Compared with the case without cold radiant panels, installing cold radiant panels at intervals along the wall can significantly reduce the temperature in the high-temperature choked region ahead of the train along monitoring line L_1, and also notably raise the temperature in the low-temperature region induced by the shock wave at the train tail. As the distance between the air and the tube wall increases, the effect of the cold radiant panels on the air temperature in the far-field region becomes negligible. This is partly because the high-temperature zone in front of the high-speed moving train sweeps across the tube wall instantaneously, resulting in a short effective time for radiative heat transfer. On the other hand, the spatial thermal resistance of radiative heat transfer increases with the growing distance between the air and the cold radiant wall, so that the temperature level of the existing cold radiant panels is insufficient to affect the air temperature at relatively distant locations.

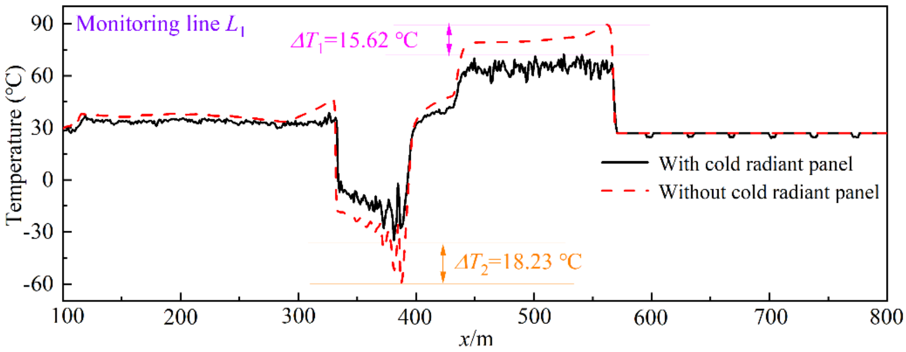

Figure 11: Temperature comparison at monitoring line L_1 with and without cold radiant panels on the wall.

Figure 12 presents the evolution laws of the average air temperature and the total system heat with and without cold radiant panels. A comparative analysis reveals that, upon activating the cold radiant panels, the maximum reduction in the average air temperature inside the tube is 0.1 °C, and the total heat within the system decreases by 30.4 kJ, corresponding to a mere 1.6% reduction compared with the case without radiant cooling. This is mainly attributed to the high operating speed of the train, which results in an extremely short effective duration for radiative heat transfer. Meanwhile, the temperature in the mainstream region around the train remains nearly unchanged. Consequently, most of the thermal energy in the system is not promptly removed directly via radiative heat transfer.

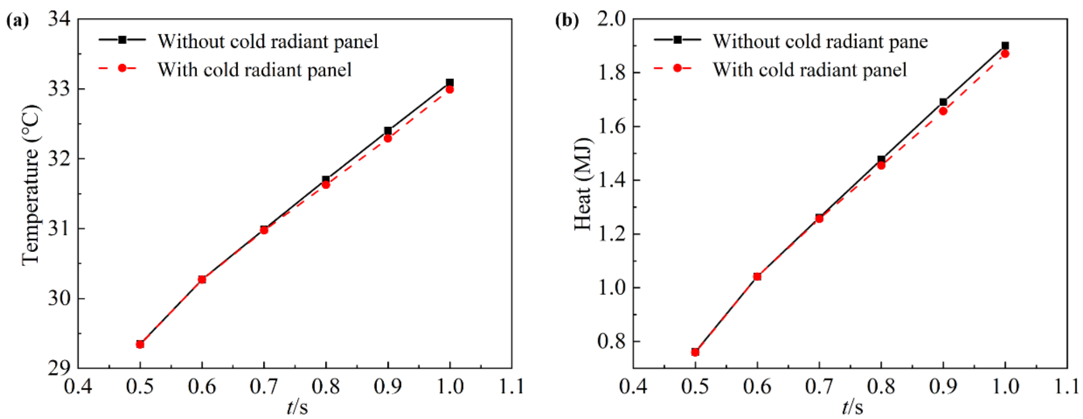

Figure 12: Comparison of average air temperature and total heat inside the tube with and without cold radiant panels.

3.3 Effect of cold radiant panel area on transient aerodynamic heating

According to the numerical results presented in Section 3.2, the current area and operating temperature of the cold radiant panel can reduce the maximum temperature on the train surface by 3.2 °C, yet such a cooling effect is relatively limited. To further improve the mitigation performance on the transient aerodynamic heat, an extended parametric study is conducted on the basis of Section 3.2 by varying the coverage area of the cold radiant panel. As illustrated in Fig. 13, the cold radiant panel is arranged along the entire length of the tube.

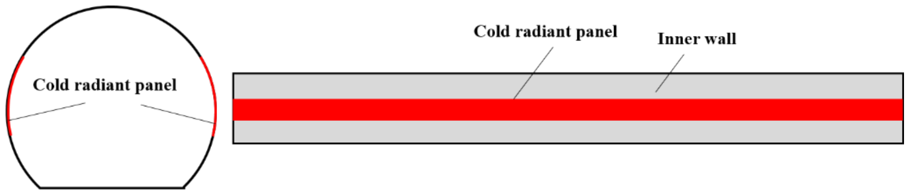

Figure 13: Schematic layout after adjusting the cold radiant panel area.

When the cold radiant panel is installed along the entire longitudinal length, the low-pressure zone and low-temperature region affected by the train-tail shock wave are reduced, whereas the high-temperature zone and high-pressure region induced by the choked flow ahead of the train remain unchanged. This indicates that adjusting the coverage area of the cold radiant panel can effectively mitigate the transient thermal environment during train operation. Subsequently, Figure 14 presents the pressure and temperature distributions along monitoring line L_3 when the cold radiant panel is laid over the full length. It can be clearly observed that, with the cold radiant panel temperature held constant, increasing its coverage area reduces the length of the low-temperature region affected by the train-tail shock wave by 8.4 m, while the length of the high-temperature choked zone ahead of the train remains unchanged, with its maximum temperature decreased by 4.1 °C. This is attributed to the expanded region influenced by radiative heat transfer as the radiant panel area increases, thereby alleviating the transient aerodynamic heating of the train.

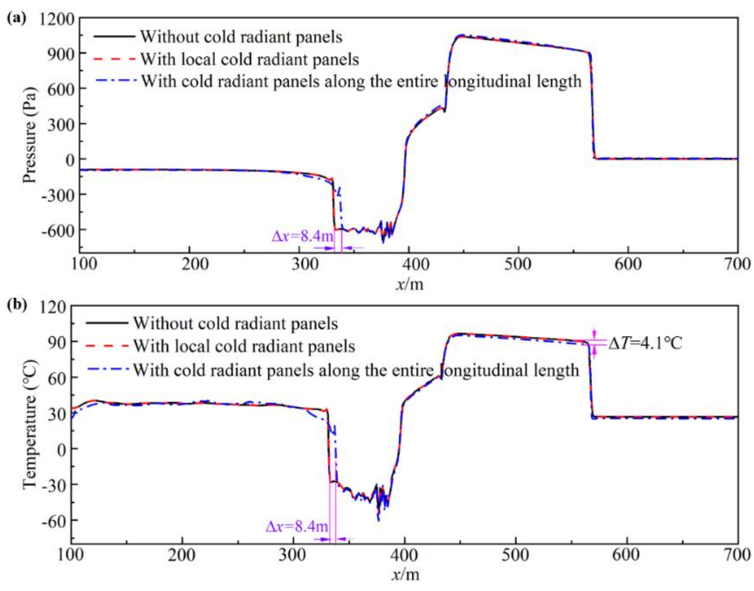

Figure 14: Effect of cold radiant panel area on pressure and temperature distributions.

Figure 15 illustrates the temperature variations on the train surface with changes in the coverage area of the cold radiant panel. When cold radiant panels are installed on the tube wall, the surface temperature of the train is reduced to a certain extent. When the cold radiant panel is arranged along the entire longitudinal length, the maximum temperature on the train surface is reduced by 12.4 °C compared with the case without radiant cooling, and by 9.1 °C compared with the case of partial panel layout. The above numerical results demonstrate that optimizing the coverage area of the cold radiant panel can effectively enhance the mitigation effect on transient aerodynamic heating inside the tube.

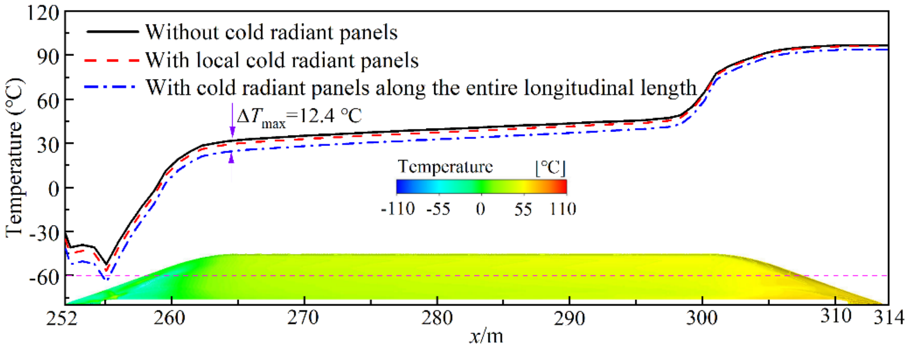

Figure 15: Temperature comparison on the train surface with different cold radiant panel areas.

4 Conclusions and Contributions

In this study, a three-dimensional numerical model is established to investigate the instantaneous aerodynamic thermal characteristics in the vacuum tube maglev train transportation system, and discuss the effect of cold radiant panels on the heat mitigation. The main conclusions are as follows:

(1) Arranging cold radiation panels on the inner wall of the tube can effectively mitigate transient aerodynamic heating during train operation.

(2) Owing to the high train speed and the short duration of radiative heat transfer, locally installed cold radiation panels reduce the maximum average air temperature in the tube by 0.1 °C, decrease the total heat within the system by 30.4 kJ, and lower the maximum train surface temperature by 3.2 °C.

(3) By increasing the coverage area of the cold radiation panels on the tube wall, the shock wave length near the train tail is shortened, which further enhances the transient aerodynamic heating mitigation effect. Correspondingly, the maximum temperature on the train surface is reduced by an additional 12.4 °C.

The results of this paper contribute to the future engineering design of evacuated tube maglev transportation systems.

Acknowledgements

The authors would like thank Research Center for Super-High-Speed Evacuated Tube Maglev Transport SWJTU and National Supercomputing Center in Chengdu.

References

[1] X. Hu, Y. Wan, Y. Mei, et al., "Wake dynamics and three-dimensional shock wave morphology in an evacuated tube transportation system under choked flow via proper orthogonal decomposition with domain partitioning", Physics of Fluids, 37(4), 2025. doi:10.1063/5.0260704

[2] Y. Sui, Q. Yu, J. Niu, et al., "Flow characteristics and aerodynamic heating of tube trains in choked/unchoked flow: A numerical study", Journal of Thermal Science, 32(4), 1421-1434, 2023. doi:10.1007/s11630-023-1806-y

[3] X.Y. Chen, L.F. Zhao, J.Q. Ma, Y.S. Liu, "Aerodynamic simulation of evacuated tube maglev trains with different streamlined designs", Journal of Modern Transportation, 20, 115-120, 2012. doi:10.1007/BF03325788

[4] Y.F. Bi, H.Q. Bi, H.L. Wang, Y.L. Zhou, J.Z. Yang, Y. Jiang, N. Zhang, "Numerical study on the effect of temperature and scale ratio on aerodynamics of maglev trains moving dynamically in a vacuum transportation system", Journal of Central South University, 2025. doi:10.1007/s11771-025-6063-7

[5] Y. Sui, J.Q. Niu, Y.P. Yuan, Q.J. Yu, X.L. Cao, D. Wu, X.F. Yang, "An aerothermal study of influence of blockage ratio on a supersonic tube train system", Journal of Thermal Science, 19, 110113, 2022. doi:10.1007/s11630-020-1281-7

[6] Q.J. Yu, X.F. Yang, J.Q. Niu, Y. Sui, Y.X. Du, Y.P. Yuan, "Thermal effects on the wall surfaces of transonic evacuated tube maglev transportation", Applied Thermal Engineering, 222, 119876, 2023. doi:10.1016/j.applthermaleng.2022.119876

[7] T.T.G. Le, J. Kim, K.S. Jang, K.S. Lee, J. Ryu, "Numerical study on the influence of the nose and tail shape on the aerodynamic characteristics of a hyperloop pod", Aerospace Science and Technology, 121, 107362, 2022. doi:10.1016/j.ast.2022.107362

[8] S.J. Bao, X. Hu, J.K. Wang, T.H. Ma, Y.Y. Rao, Z.G. Deng, "Numerical study on the influence of initial ambient temperature on the aerodynamic heating in the tube train system", Advances in Aerodynamics, 2, 28, 2020. doi:10.1186/s42774-020-00053-8

[9] Q.L. Li, W.G. Jia, C.G. Dong, R.X. Duan, "Numerical research of thermal-pressure coupling effect on blockage ratio in the evacuated tube transportation system", Key Engineering Materials, 561, 454-459, 2013. doi:10.4028/www.scientific.net/KEM.561.454

[10] Q. Yu, X. Yang, J. Niu, Y. Sui, Y. Du, Y. Yuan, "Aerodynamic thermal environment around transonic tube train in choked/unchoked flow", International Journal of Heat and Fluid Flow, 92, 108890, 2021. doi:10.1016/j.ijheatfluidflow.2021.108890

[11] Q. Yu, X. Yang, J. Niu, Y. Sui, Y. Du, Y. Yuan, "Theoretical and numerical study of choking mechanism of fluid flow in hyperloop system", Aerospace Science and Technology, 121, 107367, 2022. doi:10.1016/j.ast.2022.107367
[12] X. Hu, Z.G. Deng, J.W. Zhang, W.H. Zhang, "Effect of tracks on the flow and heat transfer of supersonic evacuated tube maglev transportation", Journal of Fluids and Structures, 107, 103413, 2021. doi:10.1016/j.jfluidstructs.2021.103413
[13] Z. Zhou, C. Xia, X. Du, et al., "Impact of the isentropic and Kantrowitz limits on the aerodynamics of an evacuated tube transportation system", Physics of Fluids, 34(6), 2022. doi:10.1063/5.0090971
[14] X.H. Zhang, Y. Jiang, T. Li, "Effect of streamlined nose length on the aerodynamic performance of a 800 km/h evacuated tube train", Fluid Dynamics & Materials Processing, 16(1), 67-76, 2020. doi:10.32604/fdmp.2020.07776
[15] J.Q. Niu, Y. Sui, Q.J. Yu, et al., "Comparative numerical study of aerodynamic heating and performance of transonic hyperloop pods with different noses", Case Studies in Thermal Engineering, 29, 101701, 2021. doi:10.1016/j.csite.2021.101701
[16] F. Xie, F. Jiang, Q. Yu, J. Niu, "Aerodynamic heating of evacuated tube transportation in choked flow under coupled forced convection and surface radiation", Journal of Wind Engineering and Industrial Aerodynamics, 269, 106333, 2026. doi:10.1016/j.jweia.2026.106333
[17] L.D. Kayser, F. Whiton, "Surface pressure measurements on a boattailed projectile shape at transonic speeds", Aberdeen Proving Ground, Maryland: Ballistic Research Laboratory, 1982.
[18] A.J. Lang, D.P. Connolly, G.D. de Boer, S. Shahpar, B. Hinchliffe, C.A. Gilkeson, "Benchmark problems for simulating hyperloop aerodynamics", Physics of Fluids, 36, 106116, 2024. doi:10.1063/5.0229914